Int. J. Heat Mass Transfer. Vol. 34, No. 2, pp. 543–558, 1991
Printed in Great Britain

0017-9310/91 $3.00 + 0.00

Transient and stability phenomena in a double diffusive natural circulation loop

YORAM ZVIRIN
Faculty of Mechanical Engineering, Technion, I.I.T., Haifa 32000, Israel

(*Received* 18 *August* 1989 *and in final form* 17 *April* 1990)

Abstract—A comprehensive work has been performed by a numerical method to study the transient and stability characteristics of a double diffusive natural circulation loop. The behaviour of the flow in the system depends on the location of the state in the four-parameter space of the thermal and saline Rayleigh numbers, R, S, the Prandtl and inverse Lewis numbers, P, Q. The stability chart in this space, obtained earlier, includes five main regions. Numerical results are presented here for flows in each of them. The transients approach monotonically or periodically stable steady states, of convection-controlled flows, or conductive rest states with no flow, in the monotonic and global stability regions, respectively. The rest state is also established in the subcritical region, if the initial velocity is smaller than a critical one, and to a steady flow otherwise. In the supercritical region, stable periodic solutions are established instead of the rest state, and in the periodic region the loop always reaches such steady oscillations, from any initial conditions. The frequency of the oscillations increases with S and decreases with R, P and Q. The heat transfer in the loop is also investigated, and it is found that some heat can be removed during the stable periodic flow.

1. INTRODUCTION

NATURAL circulation appears in geophysical processes and energy conversion systems. It provides means for energy transfer without forcing the flow by pumps or blowers, hence its importance in such systems as emergency heat removal from nuclear reactors after a hypothetical accident. Reviews on natural circulation have been written in the last decade, e.g. refs. [1, 2]. Stability, bifurcation and chaos features make problems of natural circulation interesting from the academic point of view and careful system design is needed in practical applications. Extensive work has been done on these topics, e.g. in refs. [3–8]. Combined effects of heat and mass transfer in free convection loops, i.e. double diffusive natural circulation, has not been studied, yet, in great detail. Theoretical analyses of toroidal loops were presented in refs. [9–11] and reviewed in ref. [12].

The present paper is an extension of previous work [12]. In that work an analytical method was developed to investigate the steady-state characteristics of a loop with double diffusion and to find stability regions in the parametric space, using linear stability analysis. Here a numerical method has been used to simulate the transient loop behaviour in each of these regions. Results are shown for the development of small perturbations of the rest state and for transitions from forced to natural circulation. In all cases the transients lead to stable system modes: steady flows, rest state or periodic oscillations, depending on the system parameters. In some of these the results confirm previous observations, mainly where the steady flows or rest states are approached monotonically or oscillatory in the corresponding stability domains. The present paper focuses on new results for the less familiar stability regions in the parametric space: rest states which are linearly stable but steady flows exist for them and unstable rest states without steady flow solutions. A new result is the discovery of a subzone where the long-range solution, either periodic or steady flow, depends on the initial conditions. The dynamics of the double diffusive processes leading to all these phenomena are explained. More results, demonstrating various effects, are presented and discussed in ref. [13].

2. THE THEORETICAL MODEL—STEADY SOLUTIONS AND STABILITY

The loop under consideration is shown in Fig. 1. It consists of two vertical insulated channels between two well mixed containers, where the temperatures and salinities are maintained constant, t_D, s_D at the bottom and t_U, s_U at the top. Although this is a simple system, it can serve to gain understanding about double diffusive processes occurring in channels connecting large mixed bodies of fluids, such as acquifers, important for the application of compressed air energy storage and reactor cooling loops, either gas or liquid, with penetration of impurities after a hypothetical accident. It is believed that the effect of realistic boundary conditions compared to the idealized situation treated here, is to change the values of parameters such as critical Rayleigh numbers. However, the same stability regions and transient flow, heat and mass transfer patterns would be exhibited. This is indeed indicated by the preliminary

NOMENCLATURE

A dimensionless amplitude of oscillation
a radius of pipe
g acceleration of gravity
f friction coefficient
F_B, F_s, F_t dimensionless buoyancy force and its components, $F_B = F_t - F_s \equiv RI - SJ$
H dimensionless heat per unit area removed during one half cycle, equation (17)
I, J temperature and salinity integrals, equation (12)
K_s, K_t solute and thermal diffusivities
L height of loop
n number of grid points
P modified Prandtl number, equation (4)
Q inverse Lewis number, equation (4)
q dimensionless net heat flux removed from the sink
$\bar{q}$ dimensionless average net heat flux removed from the sink during long-term stable oscillations, equation (16)
R modified thermal Rayleigh number, equation (4)
R_C critical thermal Rayleigh number, for steady-state flows
R_D critical thermal Rayleigh numbers, region D of Fig. 3
R_M, R_O critical thermal Rayleigh numbers, for monotonic and oscillatory instabilities
S modified saline Rayleigh number, equation (4)
s salinity
T dimensionless time
t temperature
U initial dimensionless velocity
V dimensionless velocity
W, $\tilde{W}$ dimensionless stable and unstable steady-state velocities
Y dimensionless location of a fluid particle emerging from the bottom container, after one half cycle, equation (17)
Z dimensionless vertical coordinate.

Greek symbols
β_s, β_t saline and thermal expansion coefficients
θ dimensionless temperature
λ, μ numerical coefficients, equation (10)
ν kinematic viscosity
ρ density
τ period of oscillation
ϕ dimensionless salinity
ω dimensionless frequency of oscillation.

Subscripts
D lower container
i at location Z_i
U upper container
1,2 channels with upward and downward flows (Fig. 1 and equations (2)).

Superscripts
j at time T^j
* bifurcation of oscillatory and monotonic marginal stability lines.

theoretical results of ref. [14], for a square loop which could be constructed and tested in a laboratory.

A one-dimensional model is adopted and use is made of the Boussinesq approximation, where the density is taken as constant in the governing equations except the gravity term in the momentum equation; there ρ is linearly related to the temperature and salinity. Laminar flow is considered, because most of the interest here is in development of flow from rest. Thus also the above boundary conditions are realistic, surface tension effects and local pressure drops at the ends of the channels are neglected and the friction coefficient is taken to be $f = 16/Re$, where Re is the Reynolds number. Mertol *et al.* [15] performed a transient two-dimensional analysis of a toroidal loop. They found that during the initial stages of flow developing from rest with a rather small Rayleigh number, rapidly decaying fluctuations of f occur around and close to an average value of nearly $16/Re$. For higher Rayleigh numbers $fRe > 16$, showing that the use of forced flow correlations in natural circulation models is not accurate. However, little is known about friction and heat transfer correlations for loops of other geometries, especially for transients, and it is surmised that the effects of changes of f are generally similar to those of different boundary conditions, as discussed above.

The equations governing the problem were written in ref. [12]. Their dimensionless form is obtained by normalizing length by L, velocity by K_t/L, time by $a^2/8\nu$, and temperature and salinity differences by $(t_D - t_U)$ and $(s_D - s_U)$. The momentum equation is integrated around the loop to eliminate the pressure term, and in the energy and diffusion equations the axial conduction and diffusion terms are kept

$$\frac{dV}{dT} = R\int_0^1 (\theta_1 - \theta_2)\,dZ - S\int_0^1 (\phi_1 - \phi_2)\,dZ - V \tag{1}$$

$$P\frac{\partial\theta}{\partial T} \pm V\frac{\partial\theta}{\partial Z} = \frac{\partial^2\theta}{\partial Z^2} \tag{2a}$$

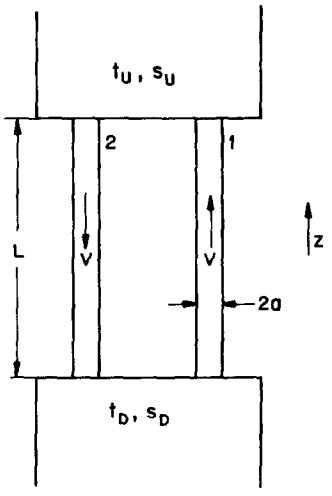

FIG. 1. A schematic description of the double diffusive natural circulation loop.

$$P\frac{\partial\phi}{\partial T} \pm V\frac{\partial\phi}{\partial Z} = \frac{1}{Q}\frac{\partial^2\phi}{\partial Z^2} \tag{2b}$$

(+ and − denote upward and downward flow in channels 1 and 2). The boundary conditions are

$$\theta = 1, \quad \phi = 1 \quad \text{at} \quad Z = 0$$
$$\theta = 0, \quad \phi = 0 \quad \text{at} \quad Z = 1. \tag{3}$$

For the transient flows, initial conditions for V, $\theta_{1,2}(Z)$ and $\phi_{1,2}(Z)$ are also specified. The dimensionless parameters of the problem are the modified Rayleigh numbers for temperature and salinity, modified Prandtl number and inverse Lewis number

$$R = g\beta_t(t_D - t_U)La^2/16\nu K_t$$
$$S = g\beta_s(s_D - s_U)La^2/16\nu K_t$$
$$P = 8(L/A)^2\nu/K_t, \quad Q = K_t/K_s. \tag{4}$$

It is noted that the time scale here is different from that in ref. [12], thus P appears in equations (2) and not in the momentum equation. However, the steady-state solution and marginal stability curves obtained in ref. [12] do not change. It follows from the continuity equation that the velocity depends on the time only, $V = V(T)$. A negative value of V means reverse flow in the loop. The equations have always (for any value of the system parameters) a no-flow solution, also referred to as conductive or rest solution

$$V = 0, \quad \theta_1 = \theta_2 = \phi_1 = \phi_2 = 1 - Z. \tag{5}$$

Convective steady flow solutions also exist

$$\theta_1 = \frac{e^{VZ} - e^{V}}{1 - e^{V}}; \quad \theta_2 = \theta_1(Z; -V) \tag{6a}$$

$$\phi_1 = \frac{e^{QVZ} - e^{QV}}{1 - e^{QV}}; \quad \phi_2 = \phi_1(Z; -QV) \tag{6b}$$

where the velocity is given by the solution of the algebraic equation

$$R\left(\frac{e^{V}+1}{e^{V}-1} - \frac{2}{V}\right) - S\left(\frac{e^{QV}+1}{e^{QV}-1} - \frac{2}{QV}\right) = V. \tag{6c}$$

Steady-state results are presented in ref. [12]. An example is shown here in Fig. 2 with some new results for higher Rayleigh numbers. It can be seen that the solution does not depend on P, and that for thermal Rayleigh numbers below a critical value $R_C(Q, S)$ there does not exist a steady flow. In the region $R_M(Q, S) \geqslant R \geqslant R_C$ there are two solutions and for $R > R_M$ only one. The multiplicity of the steady-state solution is larger, because for any one with velocity W, the mirror image flow $-W$ is also a solution (there is no preference to any channel). Thus, for example, there are five solutions in the region $R_M \geqslant R \geqslant R_C$.

A linear stability analysis was performed in ref. [12]. It showed that all the convective solutions on the lower branches of the curves of $V(R; S; Q)$, i.e. $\tilde{W}$, see Fig. 2, are unstable for small perturbations, while all the solutions on the upper branches, W, are stable. Results of the stability investigation of the rest state are reproduced, again, from ref. [12] in Fig. 3 as a chart in the R–S plane for $Q = 2$ and $P = 1$. The chart depends on the Prandtl and Lewis numbers, as shown in ref. [12]. Two types of boundary curves were revealed; the first is a monotonic marginal stability line (MMSL), which coincides with R_M

$$R = R_M = 6 + QS. \tag{7}$$

Small disturbances should grow for $R > R_M$ and decay for $R < R_M$, monotonically. This line does not depend on P. The other line is an oscillatory marginal stability line (OMSL), $R_O(S; Q, P)$, which branches off from the MMSL at the point S^*, R^* shown in Fig. 3. Small perturbations should grow in an oscillatory mode for $R > R_O$ and decay in this mode for $R < R_O$. The frequencies of the critical perturbations, associated with points on the lines R_O, were found in the analysis of ref. [12] but not included in that reference. They are listed in Table 2 of ref. [13], and for $Q = 2$, $P = 1$ in Table 1 here. It is shown in refs. [12, 13] that the lines R_O for various values of P intersect each other and also the line R_C.

The general analytical results of ref. [12] show that for any value of the inverse Lewis number, Q, and the modified Prandtl number, P, the marginal stability lines R_M and R_O and the critical Rayleigh number R_C divide the S–R plane into five main stability regions for small disturbances, as illustrated in Fig. 3. Region A is that of global instability, where a perturbation should grow monotonically. Region B is that of stability, where every small disturbance should decay (monotonically below R_M and with oscillations below R_O), and there does not exist a steady flow in the loop. In region D $R_M > R > R_C$ and $R > R_O$. Here a perturbation should grow in an oscillatory mode, and four convective solutions exist, two stable ($\pm W$) and

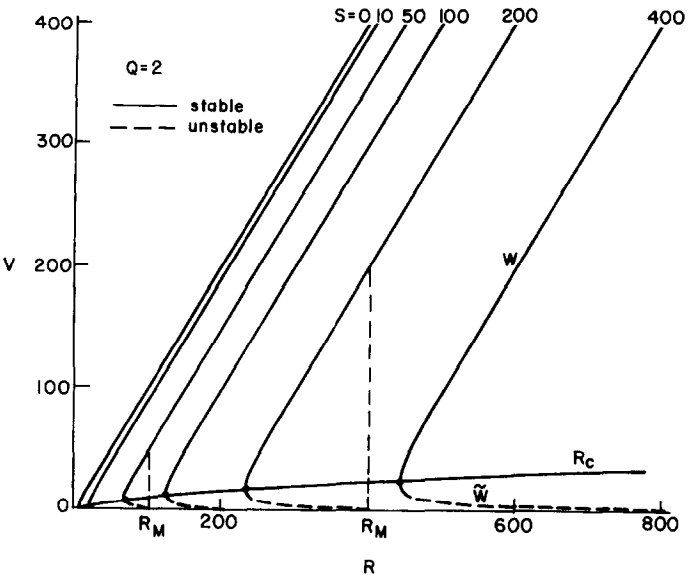

FIG. 2. Dimensionless steady-state velocity, V ('convective solution'), as a function of the thermal Rayleigh number, R, for various values of the saline Rayleigh number, S. The inverse Lewis number is $Q = 2$.

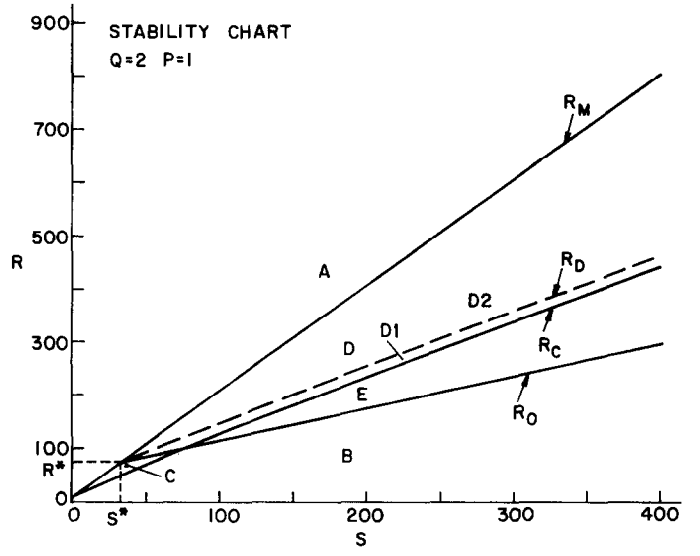

FIG. 3. Stability chart in the Rayleigh numbers plane, $S-R$, for the inverse Lewis number $Q = 2$ and the Prandtl number $P = 1$. The stability regions are: A, monotonic instability; B, global stability; C, subcritical instability; D, supercritical instability; E, periodic.

two unstable ($\pm \tilde{W}$). This region is called supercritical instability. It has been found here from the numerical results that it can be divided into two sub-zones, D1, D2 by the line R_D. The characteristics of these sub-zones are presented and discussed in Section 4.3 below. In region C, the steady solutions exist, again, but small perturbations should decay (monotonically or with oscillations). This situation is referred to as subcritical instability, and it is implied that larger disturbances would develop with non-linear effects until a steady flow be established. In region E, where $R_C > R > R_O$, small disturbances should grow but no steady flows exist. It was postulated in ref. [12] that here non-linear effects take-over at some time, "leading to either a decay to the rest state or to transient behaviour, possibly of a 'chaotic' type".

The transient analysis performed in the present work and described in the following sections, validates, indeed, all these flow types in the various stability regions. Quantitative results are presented for the velocity, temperature and salinity fields $V(T)$, $\theta_{1,2}(Z, T)$ and $\phi_{1,2}(Z, T)$, depending on the system

Table 1. Frequency of oscillations on the oscillatory marginal stability line R_O of Fig. 3: $P = 1$, $Q = 2$

S	R	W	S	R	W
33	72	0	150	141.2	9.138
33.5	72.30	0.600	175	156.3	10.04
34	72.58	0.855	200	171.6	10.86
34.5	72.87	1.047	250	202.5	12.33
35	73.16	1.209	300	233.9	13.61
36	73.73	1.481	350	265.6	14.77
38	74.89	1.912	400	297.6	15.83
39	75.47	2.094	450	330.0	16.81
40	76.05	2.262	500	362.6	17.72
42	77.21	2.564	600	428.8	19.39
44	78.37	2.834	700	495.9	20.90
46	79.53	3.080	800	563.8	22.29
48	80.69	3.309	900	632.4	23.57
50	81.96	3.521	1000	701.7	24.77
55	84.77	4.002	1500	1055	29.91
60	87.69	4.432	2000	1417	34.14
65	90.61	4.822	2500	1784	37.82
70	93.54	5.183	3000	2154	41.15
80	99.42	5.835	4000	2896	47.06
90	105.3	6.418	5000	3640	52.33
100	111.2	6.951	6000	4381	57.15
110	117.2	7.444	7000	5120	61.64
120	123.2	7.904	8000	5856	65.86
130	129.1	8.337	9000	6589	69.86
140	135.2	8.747	10000	7320	73.67

parameters R, S and on initial conditions. The effects of Q and P were studied by ref. [13] and the main results are reviewed below. Frequencies of the oscillatory patterns are also found. For regions E and D1 it is shown that periodic oscillations with constant frequencies and amplitudes are established, which are not monochromatic, i.e. not simple harmonic.

3. THE NUMERICAL METHOD

The transient solution of equations (1)–(3) is performed by the implicit finite differences method described below. It is based on the Crank–Nicholson method to solve the P.D.E. (2), and the modified Euler method to solve the O.D.E. (1), where the integrations are carried out by the Simpson quadrature.

The equations are written as

$$\left(\frac{\partial\psi}{\partial T}\right)_i \cong \frac{\psi_i^{j+1}-\psi_i^j}{\Delta T} = \tfrac{1}{2}(\mathrm{RHS}^{j+1}+\mathrm{RHS}^j)_i;$$

$$\psi = V, \theta_{1,2}, \phi_{1,2} \quad (8)$$

for any point Z_i and time interval (T^j, T^{j+1}). Central differences are taken for the first and second spatial derivatives, on the right-hand sides of the equations. This procedure leads to the tri-diagonal system of linear algebraic equations, representing equation (2a)

$$-(\mu+\lambda V^{j+1})\theta_{1,i-1}^{j+1}+(1+2\mu)\theta_{1,i}^{j+1}$$
$$+(-\mu+\lambda V^{j+1})\theta_{1,i+1}^{j+1} = (\mu+\lambda V^j)\theta_{1,i-1}^j+(1-2\mu)\theta_{1,i}^j$$
$$+(\mu-\lambda V^j)\theta_{1,i+1}^j, \quad i = 1,2,3,\ldots,n-1 \quad (9)$$

where n is the number of grid points, i.e. $n = 1/\Delta Z$

$$\mu \equiv \frac{\Delta T}{2P(\Delta Z)^2}, \quad \lambda \equiv \frac{\Delta T}{4P\Delta Z}. \quad (10)$$

The finite differences form of equation (2b) for θ_2 is obtained by introducing in equation (9) $-\lambda$ instead of λ. Similarly, μ/Q and $\pm\lambda$ are inserted in equation (9) for $\phi_{1,2}$. The form (8) for equation (1) leads to

$$V^{j+1} = \frac{1}{1+\Delta T/2}\left\{\left(1-\frac{\Delta T}{2}\right)V^j + \frac{\Delta T}{2}[R(I^{j+1}+I^j)-S(J^{j+1}+J^j)]\right\} \quad (11)$$

where

$$I = \int_0^1 (\theta_1-\theta_2)\,\mathrm{d}Z; \quad J = \int_0^1 (\phi_1-\phi_2)\,\mathrm{d}Z. \quad (12)$$

It is noted that the problem is nonlinear and V^{j+1} is not known a priori on the left-hand side of equation (9). Therefore, the following iterative procedure is used, for any time step:

(1) V^j, θ_i^j and ϕ_i^j are known from the solution for the previous time step (and from the initial conditions for the first one).

(2) A value for V^{j+1} is chosen as a first guess.

(3) Equations (9) are solved by the Thomas algorithm to get the fields $\theta_{1,2}^{j+1}$, $\phi_{1,2}^{j+1}$.

(4) These fields are used to calculate the integrals I, J (equation (12)) and a new value V^{j+1} is computed by equation (11).

(5) Steps 3 and 4 are repeated iteratively until convergence of V^{j+1} to the required accuracy is achieved.

(6) Convergence of $\theta_{1,2}^{j+1}$, $\phi_{1,2}^{j+1}$ is checked and steps 3–5 are repeated if necessary.

This double-nested iterative procedure is obviously implicit, and convergence has been obtained quite comfortably in all the cases investigated here. The solution was performed on the Technion IBM 3081 computer, by a program developed in this work. A few examples are given in ref. [13] for the convergence patterns as a function of the grid size and time step, ΔZ and ΔT, for both monotonic and oscillatory transients. Most of the results presented in the following sections are for $V(T)$. The numerical parameters in each case were chosen so as to achieve an accuracy of 0.1% for the velocity, except for cases with large values of R ($R \geqslant 400$) where accuracies of a maximum of 1.5% or less were maintained, in order to save computer time and memory.

4. RESULTS AND DISCUSSION—VELOCITY, TEMPERATURE AND SALINITY FIELDS

4.1. *Initial conditions: instability and stability regions A, B*

The computer program was used to obtain transient results for many cases in a wide range of the par-

ameters R, S, P and Q, and for many types of initial conditions (ICs). Results are shown here mainly for the following two IC types, which appear more frequently in practical applications. (a) An initial condition of the rest state (conductive solution with no flow), where the temperature and salinity distributions are linear, equation (5). A small initial velocity, $U = 0.01$ in most cases, is imposed at $T = 0$. This transient is called here NF. (b) Initial velocities U which are not small, with θ and ϕ profiles given by inserting $V = U$ in equations (6). These transients, referred to as FF in the following, are transitions from initial steady forced flow to natural circulation, for example by shutting off the driving pump at $T = 0$. Other ICs studied in the present work include additional finite velocities $0 \leqslant U \leqslant 100$, with the rest θ and ϕ distributions or the unbalanced profiles $\theta_1 = \phi_2 = 1$, $\theta_2 = \phi_1 = 0$, and other very small perturbations, e.g. $U = 0$ and θ and ϕ given by the conductive solution (5) except for a local deviation at one point only: $\theta_1(\Delta Z) = \phi_1(\Delta Z) = 1$.

It was found that the qualitative behaviour of the solution within each of the stability regions A–E in Fig. 3 is similar, the values of the parameters affect only the transition between the regions and the quantitative solution (i.e. absolute values of the velocity, temperature and salinity and amplitude and frequency of oscillations). Numerous solutions have been inspected; we have chosen to concentrate on presenting results for single values of the Prandtl and Lewis numbers: $Q = 2$, $P = 1$, and to show the effect of the Rayleigh numbers R and S. This corresponds to working with the same fluid and changing (e.g. in experiments) the parameters R and S, which can be controlled by imposing temperature and salinity differences. Reference [13] includes more results for all the stability zones A–E and also several examples for other values of P and Q and other ICs.

As mentioned above, the present paper focuses, for brevity, on the less familiar and more interesting stability regions. Therefore, for regions A and B of Fig. 3 only general trends are summarized. The results for the global stability region A show that the steady-state flow is approached monotonically from any initial condition. The rate of the transient is faster when the destabilizing Rayleigh number, R, increases and the stabilizing S decreases, as expected. FF transients hardly depend on Q and strongly on P, in different manners which vary with R and S.

The transients studied in the stability region B of Fig. 3 always decay to rest, regardless of the IC, either monotonically or oscillatory (depending on the location relative to the marginal lines R_O and R_M). This seems to indicate that region B is of global stability, where any initial flow is attracted to the conductive solution. This deduction is strengthened by the analytical results of refs. [9, 10], which showed the existence of a global stability zone for a loop model without heat and mass diffusion, which tend to stabilize the system.

4.2. *Subcritical instability region*, C

Region C in Fig. 3 ($R_C \leqslant R \leqslant R_M$, R_O) is that of subcritical instability, i.e. small perturbations to rest should decay (for states below either the MMSL or the OMSL) and four steady convective solutions exist: stable $\pm W$ and unstable $\pm \tilde{W}$ (see Fig. 2). It has been found, indeed, from the numerical solutions, that small disturbances to the rest state in this region always decay, monotonically or with oscillations, depending on the location of the state in the region. Examples of $V(T)$ transients for states in region C are presented in Figs. 4 and 5. An interesting phenomenon has been obtained for transitions from finite initial flows: FF transients with initial velocities smaller than the unstable steady ones, $U < \tilde{W}$, always decay to the rest state, while for $U > \tilde{W}$ the stable steady flow with $V = W$ is established. Transients starting from conductive (rest) profiles of θ and ϕ by imposing a finite initial velocity U develop to steady flow solutions if at some time during the periodic process the velocity exceeds the value $\tilde{W}$. If, however, the amplitude does not reach this value, oscillatory decay to rest occurs.

Figure 4 shows FF transients in the right portion of region C, below the OMSL. For $U > \tilde{W}$, the stable convective solution is reached monotonically, both for $U > W$ and $U < W$. The stability of this final state is demonstrated in the straight horizontal line $V = W$ for $U = W$, thus the numerical disturbances do not affect this stable flow solution. When $U < \tilde{W}$, an oscillatory decay to the conductive solution ($W = 0$) is observed, as expected for points below R_O. The transient with $U = \tilde{W}$ is interesting: for a rather long time $V(T)$ is almost constant at this value, but a very small decrease finally leads to oscillations and decline to rest. It is noted that this is a feature of the numerical parameters, and a different choice could cause the solution to simulate a velocity increase. Similar patterns were observed in the left portion of region C. NF transients, obviously with $U < \tilde{W}$, always decay as shown in Fig. 5, which includes states below either R_M or R_O. Near the MMSL ($R = 26$) the oscillation consists of a strong overshoot, followed by one flat undershoot leading to rest. The other cases ($R = 30$, 39) below the OMSL, exhibit oscillatory decay. The frequency, ω, of the oscillations decreases with R and also Q, P and increases with S; the amplitude, A, increases with both R and S and also with Q, P. These trends have the same fashion as in region B, see also Fig. 14. The double diffusive dynamics of the oscillations and other flow patterns are discussed below.

Figure 5 also shows two transients with finite U and linear (rest) initial θ and ϕ profiles (for $R = 57$, $S = 26$). For the one with $U = 0.237$, A is just below $\tilde{W} = 0.646$ and oscillatory decay occurs. For the one with $U = 0.238$, monotonic increase to W commences after V reaches $\tilde{W}$. The role of $\tilde{W}$ as a critical velocity for various transients will also be seen from results for region D.

As observed from Fig. 5 and from the results of ref. [13], the decay to rest is slower when the state

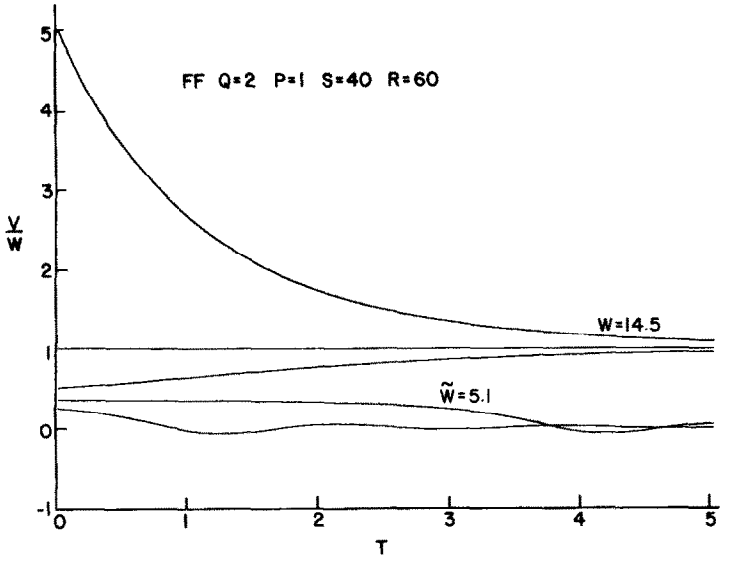

FIG. 4. FF transients, region C of Fig. 3. Monotonic transition to steady state for $U > \tilde{W}$, oscillatory decay when $U \leqslant \tilde{W}$.

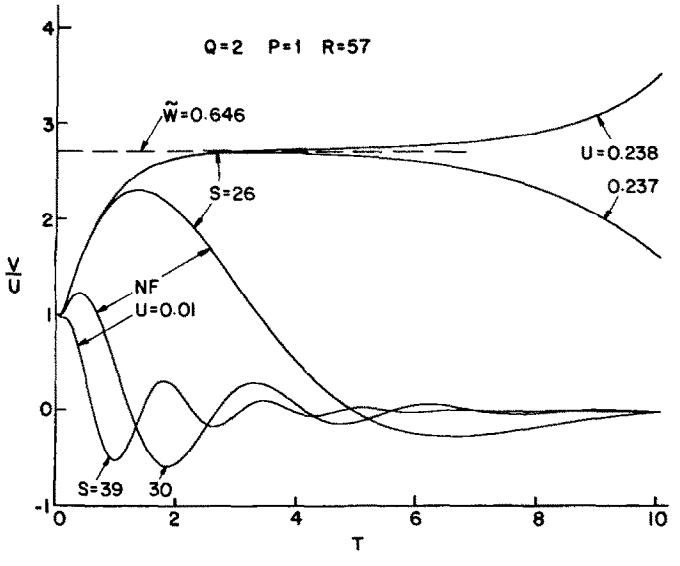

FIG. 5. NF transients, region C of Fig. 3, decaying oscillations for $S > 30$, monotonic decay after one large oscillation for $S = 26$; growing and decaying finite initial disturbances.

approaches the marginal stability line R_M or R_O, i.e. when the driving buoyancy force rises by increasing R and decreasing S. It is interesting to note that the amplitude of the decaying oscillations of NF transients can be much larger than the initial velocity. This is seen in Fig. 5, and for $R = 72$, $S = 34$ it was found that the amplitude is $\sim 3U$ with a small frequency and very slow decay rate.

4.3. *Supercritical oscillatory instability region*, D

Region D in the stability chart (Fig. 3), where $R > R_O$ and $R_C \leqslant R \leqslant R_M$, is that of supercritical instability: small perturbations tend to grow and four steady flow solutions exist with $\pm W$, $\pm \tilde{W}$. The numerical results show that NF transients, starting from small disturbances to rest, always develop to convective flows: either to one of the stable steady ones $\pm W$ or to a stable periodic flow. Obviously the latter could not be found by the steady analysis of ref. [12]. Examples of all these patterns are presented in Figs. 6–10 and discussed in the following.

Two different patterns have been discovered, for two sub-zones of region D. In the first one, D1, $R > R_O$ or $R > R_C$ and $R < R_D$ ($R_D \approx 101.8$ for $S = 60$ and $R_D \approx 465$ for $S = 400$), the small disturbance develops to a periodic stable flow, with constant amplitude and frequency, which is not monochromatic (Figs. 6–9). The shape of the cycle

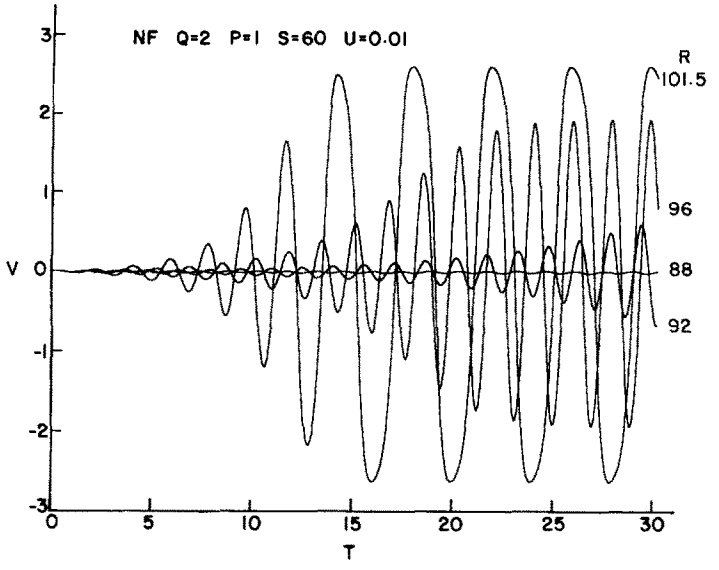

FIG. 6. NF transients, region D1 of Fig. 3, effect of R on periodic solution.

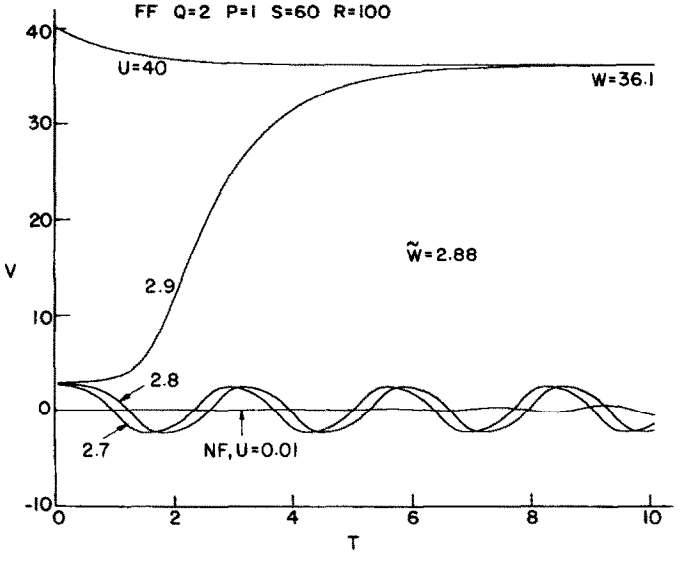

FIG. 7. FF and NF transients, region D1 of Fig. 3, effect of the initial conditions.

becomes more skewed for large S and R, as demonstrated in Fig. 9. A increases and ω decreases when R rises and S is lowered, as for the decaying oscillations in regions B and C. However, here the period of the growing oscillations increases with time, thus the frequency decreases until the stable periodic flow with constant ω is established. When R rises above the critical value R_D, we cross to the second sub-zone of region D, D2, where $R_D < R < R_M$. As seen in Figs. 8 and 10, the small oscillations grow periodically, with decreasing ω, again, and then at the point when $V(T)$ reaches the critical level, $\tilde{W}$, a complete change occurs and a monotonic growth commences, leading to the steady-state flow with W or $-W$, depending on the sign of V where the switch takes place. This depends on the initial conditions as shown in Fig. 10. Here for the larger R (116), the small perturbation seems to grow monotonically to the steady flow. However, a closer look at the initial stage of the transient reveals that the small velocity perturbations decrease, first, and only then start growing. This happens because the state is below the MMSL, so a small disturbance tends to decay, but since the state is significantly above the OMSL, the conductive solution is unstable. Thus the flow picks up again, before the velocity changes sign, accelerates and approaches the steady convective solution, without oscillations. A similar process was found to occur for the IC with

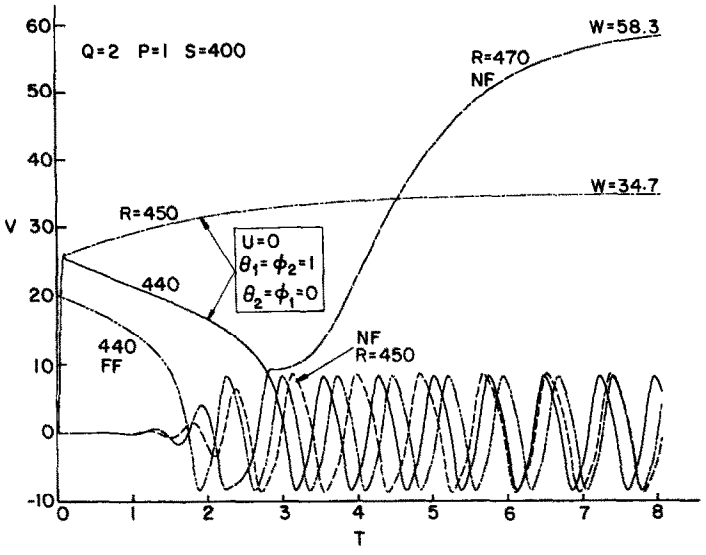

FIG. 8. NF transients, regions D1 ($R = 450$), D2 ($R = 470$) and E ($R = 440$) of Fig. 3, effects of R and the initial conditions.

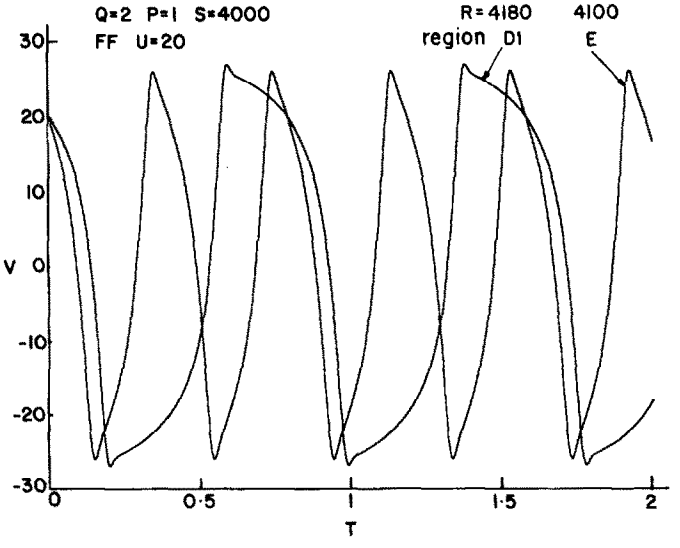

FIG. 9. Oscillatory solutions for large Rayleigh numbers in regions D1 and E of Fig. 3.

$U = 0$ and tiny local perturbations to the rest profiles of θ and ϕ, except here a few oscillations may first appear.

Figure 7 illustrates both FF and NF transients in sub-zone D1, leading to either the periodic or the steady solution, for various initial velocities, U. Several interesting phenomena are exhibited in these results. As can be seen here, two different FF processes can emerge, depending on whether the initial forced flow velocity, U, is larger or smaller, again, than the unstable steady one $\tilde{W}$: monotonic approach to the steady flow, W, in the former situation or development of a stable periodic flow in the latter. This is also observed for the NF transient (small U) in Fig. 7, and was found for other values of U and initial rest θ and ϕ profiles, where the steady flow is approached monotonically from the moment when V reaches the value $\tilde{W}$. As can also be seen from Fig. 7, the long-term oscillation amplitude and frequency does not depend on the initial conditions. It is noted that the NF case here reaches the fully developed periodic pattern at $T \approx 17$, longer than the final time shown.

Figure 8 describes transients in stability regions D1, D2 and E of Fig. 3. The NF transient leads to a stable periodic flow in D1 ($R = 450$), and to the steady convective solution W in D2 ($R = 470$), after V exceeds the value $\tilde{W} = 8.8$ during the oscillations. For $R = 450$ another type of IC is shown: $U = 0$ with the

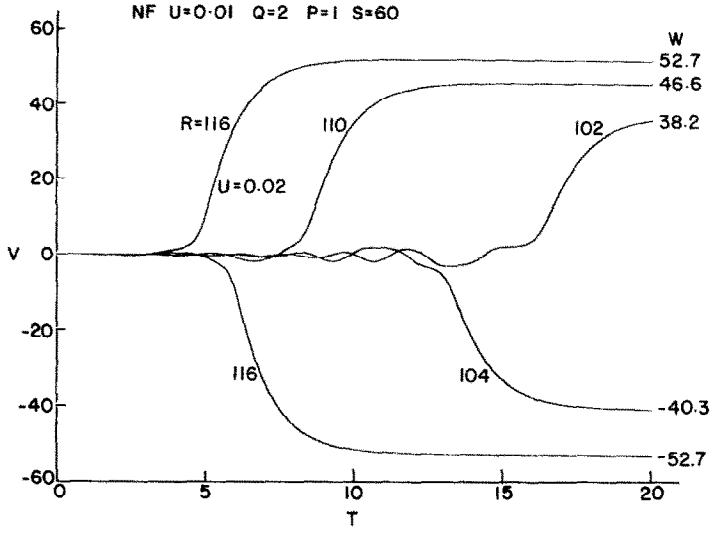

FIG. 10. NF transients, region D2 of Fig. 3, effects of R and the initial conditions on oscillatory and monotonic transitions to steady state.

unbalanced distributions $\theta_1 = \phi_2 = 1$, $\theta_2 = \phi_1 = 0$. For this finite disturbance the initial net driving force is large (strong buoyancy and weak friction at low V), and the velocity sharply rises. A balance of the forces is quickly attained, followed by a moderate approach to steady state. The same IC leads to a stable periodic flow in region E ($R = 440$), as also with the FF transient shown here and all other ICs studied. It is noted that the effect of R on the oscillations is continuous across the line R_O separating regions D and E: A decreases and ω increases when R is lowered (and when S rises). This is seen, again, in Fig. 9 which shows the skewed patterns for large R and S. As seen in Figs. 6–10, the effect of raising the destabilizing R is also to accelerate the transients: as R increases, the stable steady state, with increasing $|W|$, or the long-term stable oscillations are approached faster. A similar effect was observed for decreasing the stabilizing parameter, S, cf. ref. [13].

4.4. *Region of periodic solutions*, E

Region E in the stability chart (Fig. 3) lies above the OMSL and below R_C. Thus rest states in it are unstable and steady flows do not exist. This means that all the solutions must be time dependent, which has been confirmed, indeed, by the numerical results. In all cases, for both NF and FF transients and other IC studied, the flow exhibits developing oscillations, during which the frequency decreases with time, leading to stable periodic solutions. These have constant amplitudes and frequencies but their shape is, again, skewed (not simple harmonic) and depends on the time during the cycles.

Figures 8, 9 and 11 show the development of the periodic flows for various transients. The processes in this region progress at a slower rate than those in the other stability regions; in general, they are faster as R increases and S decreases. The initial velocity in all cases of Fig. 11 is $U = 0.1$. It was found in ref. [13] that for $U = 0.01$ and for $U = 0$ with very small local disturbances of θ and ϕ, the rate of the transients is much slower. As before, the effect of increasing R is to increase the amplitude and decrease the frequency of the stable long-term oscillations, the effect of S is opposite and the shape of the oscillations become more skewed with increasing Rayleigh numbers. This phenomenon is clearly seen in Fig. 9 for $S = 4000$, $R > 4000$.

The results in the present paper are for $P = 1$, $Q = 2$; a few examples are given in ref. [13] to show the influence of these parameters. The results show that the amplitude increases and the frequency decreases when Q and P rise, with a much sharper effect of the latter. An interesting result is that the time to establish the long-term periodic flow from a small perturbation becomes longer as Q decreases, while the rate of oscillations decay for FF transients in region B was found to be faster when Q decreases. These opposite trends hint at the difficulties encountered when attempting to explain the effects of the parameters and the physical phenomena of the nonlinear complicated problem. However, let us discuss now the double diffusive dynamics of the periodic flow.

Figure 12 demonstrates the relation between the time-dependent velocity, temperature and salinity during a stable periodic solution for $S = 400$, $R = 400$: $V(T)$ is plotted together with the temperature θ_1 and salinity ϕ_2 at mid-height of the loop ($Z = 1/2$). The initial velocity of the FF transient is $U = 7.5$, close to the amplitude of the stable oscillations. It is seen, as noted above, that there are (constant) phase shifts between V, θ and ϕ. These can cause instabilities of oscillation growth even in a

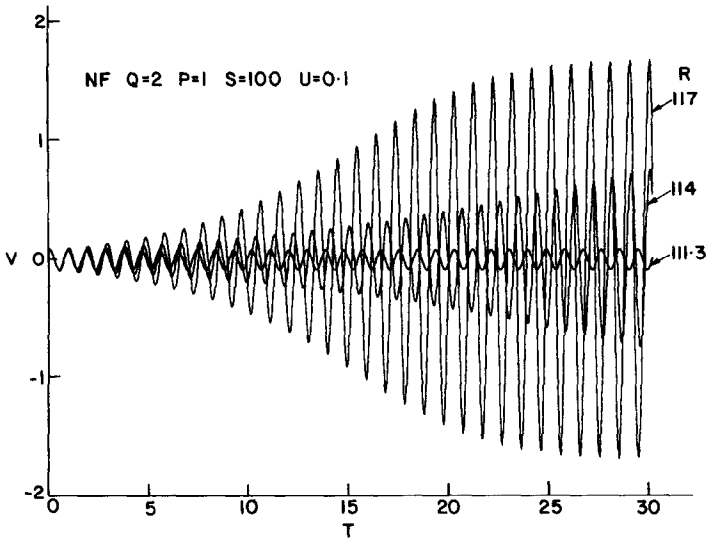

FIG. 11. NF transients, region E of Fig. 3, effect of R on periodic flow, $U = 0.1$.

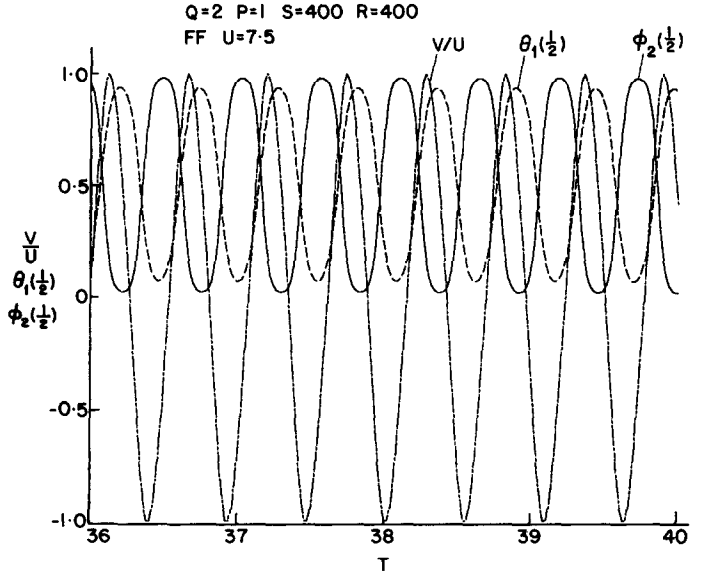

FIG. 12. Long-term stable periodic solution in region E of Fig. 3: the velocity V, the temperature θ_1 and salinity ϕ_2 at mid height of the loop; $36 \leqslant T \leqslant 40$.

single-phase single-component loop, as demonstrated by Welander [4]. In our case, the mechanisms of the double diffusive stable and unstable oscillations are explained by observing the behaviour of the forces appearing in the momentum equation (1). Figures 13(a) and (b) describe the time-dependent buoyancy force, F_B, and its components F_t, F_s, and also $V(T)$ which is the dimensionless friction force, for transients in regions E and D. $V(T)$ for these two transients is also illustrated, on a larger scale, in Fig. 8. The acceleration dV/dT is equal to the net balance force, $F_B - V$, and V increases whenever F_B exceeds the friction (V). During the oscillations in region E (Fig. 13(a)), the magnitude of the stabilizing force, F_s, is larger than that of the destabilizing one, F_t. Both grow initially, as the temperature and salinity distributions build up, and due to the phase shift between them a periodic net buoyancy force always exists, driving the fluid in growing and then stable oscillations. The cycles are not monochromatic because of the non-linearity of the effects: the mutual dependence and phase shifts between F_t, F_s and V. When R increases and we move into region D, the magnitude of the destabilizing force, F_t, becomes larger than F_s, see Fig. 13(b). The oscillations grow initially as before; in region D1 (not shown in this figure) the amplitude does not reach the critical value $\tilde{W}$ and stable periodic flow is established. In region D2 (Fig. 13(b)), V

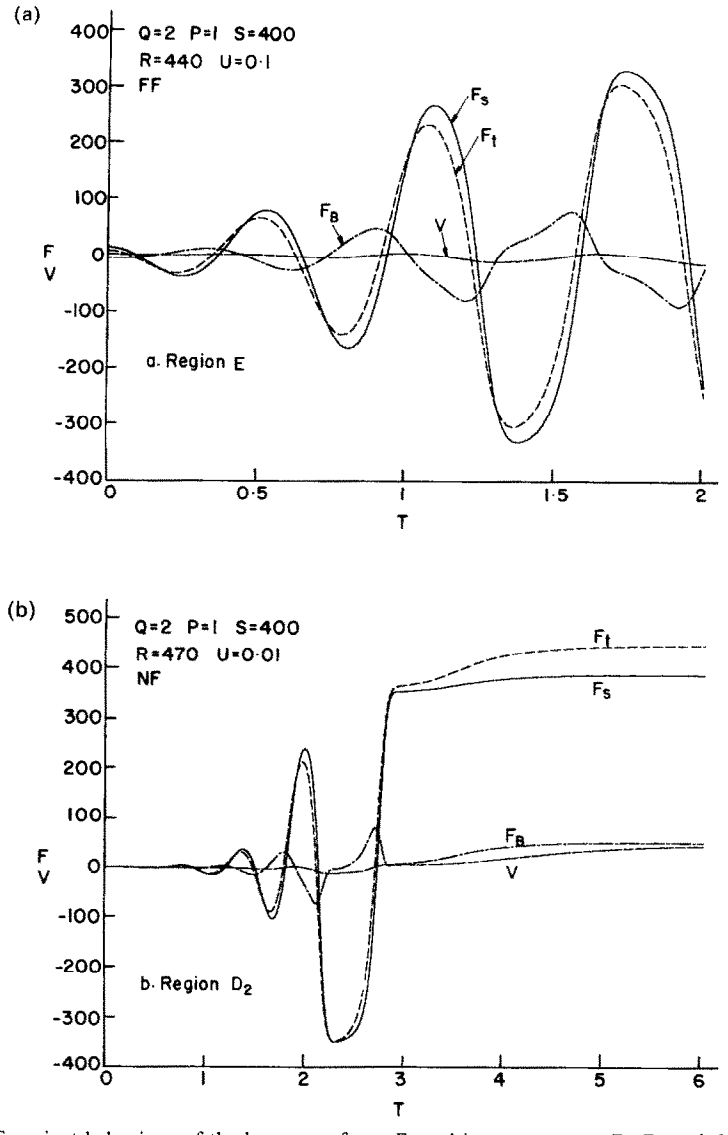

FIG. 13. Transient behaviour of the buoyancy force F_B and its components F_s, F_t, and the friction force which is equal to V: (a) region E; (b) region D2.

reaches $\tilde{W}$ at some point, and an immediate switch occurs to the stable upper solution branch seen in Fig. 2. F_t stays larger than F_s, and the driving force F_B tends to a constant value, which is equal to the friction, given by the velocity $V \to W$ (Fig. 13(b)). Thus a stable steady flow is established. Further increase of R causes the state (in the parametric space) to move above the MMSL, into the instability region A, where any disturbance grows monotonically. Decreasing R below the OMSL leads to oscillatory decay to rest. The effects of S are opposite.

All the results obtained here for regions E and D1 of the loop under consideration, show that for this system only stable long-term solutions are established: either steady or periodic ones, but no chaotic situations were detected. Such chaotic solutions were discovered, for example by Hart [11], in regions where unstable steady solutions exist with no (unpaired with) stable flows. For the present loop we have found that in cases of unstable-steady states $V = \tilde{W}$ or 0 there are also stable ones, W, and the transients lead to either the latter or to stable periodic flows.

Figure 14 shows the long-term frequency of oscillations, ω, as a function of the Rayleigh numbers. The various stability regions (where periodic flows exist) are marked in the figure as well as the marginal lines separating them. It is seen that ω increases when R is lowered and when S is raised. It changes continuously upon crossing from region to region through the lines R_O, R_D and R_C. It was also found that the frequency decreases when P and Q rise. The frequencies obtained from the numerical solutions for points on the marginal stability lines, exactly agree with the values calculated analytically in ref. [12], listed in Table 1. The theoretical limit of the frequency for R approaching the monotonic marginal stability line, R_M, from

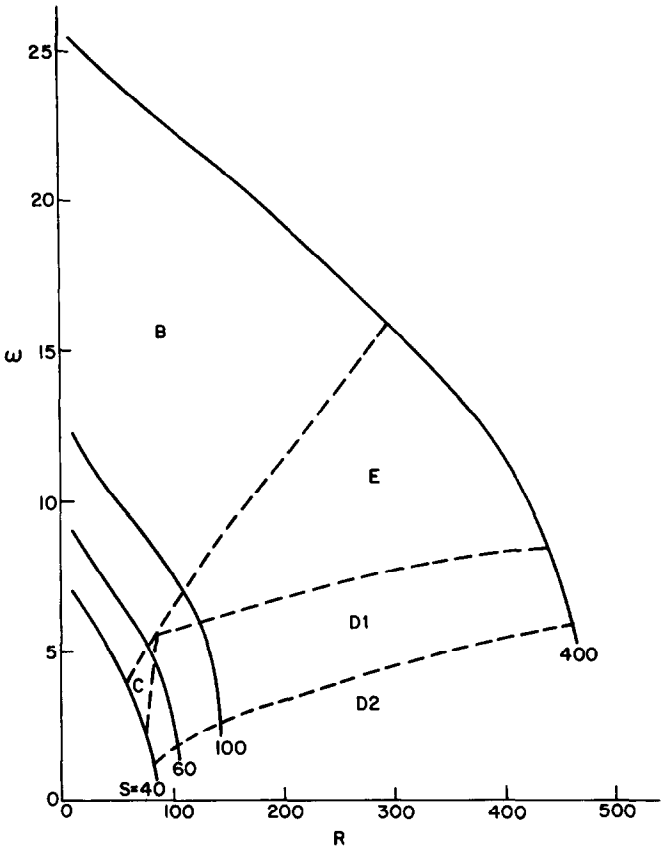

FIG. 14. Frequency dependence on the thermal and saline Rayleigh numbers R and S, in the stability regions B–E where oscillations occur. $Q = 2$, $P = 1$.

below, is obviously zero. The results of the present work show that this limit is realized only in the narrow zone near the intersection of the MMSL and OMSL, R_O. The frequency for $S = 40$ and the relatively larger R, see Fig. 14, tends, indeed, to zero. At higher values of S and R, states just below R_M are deep in the instability region D (sub-zone D2). A small disturbance to the rest state declines slightly, followed soon by non-linear effects which cause a rather quick monotonic transition to one of the two stable solutions $\pm W$.

5. RESULTS AND DISCUSSION—HEAT TRANSFER

The equations governing the velocity, temperature and salinity fields in the double diffusive loop were developed in Section 2 and solved by the numerical method outlined in Section 3. Results for these fields were presented and discussed in Section 4, for all the regions in the stability chart (Fig. 3). Here the heat transfer characteristics of the loop are studied, mainly for the purpose of evaluating the capability of the system to remove heat from the heat source in the bottom to the sink at the top.

The heat transfer is more important and of interest for the long-term system flows than for the initial stages of transients leading to them. We have observed either stable steady states or stable periodic oscillations; these two types of long-term solutions are treated in the following. Let us consider, first, stable steady flows with large velocities, at high values of the driving force, represented by the difference of the Rayleigh numbers: $R-S$. In this case $V = W \gg 1$ and the temperature distributions approach $\theta_1 = 1$, $\theta_2 = 0$ (except for small sections near the top for θ_1 and bottom for θ_2). Thus heat is transferred almost solely by convection. The heat flux between the source and the sink is proportional to the product of the velocity and the temperature difference $t_D - t_U$, or in dimensionless form

$$q = W, \quad W \gg 1. \tag{13}$$

This result can also be found from a more general and rigorous derivation. Consider a small control volume consisting of the two loop channels, between the bottom container, $Z = 0$, and a short elevation $\delta Z \to 0$. The rate of energy delivery into the heat source by the flow in the downcomer (channel 2) tends to be equal to the rate of energy convected from the source into the riser (channel 1): the velocity is the same (due to continuity) and both temperatures θ_1 and θ_2

Table 2. Average long-term heat flux for various stable periodic solutions

S	R	Region	$\tau/2$	H	$\bar{q}$	W	Y
60	100	D1	1.338	3.24	2.43	36.1	2.14
400	400	E	0.269	0.965	3.59	—	1.22
4000	3000	E	0.0656	0.300	4.57	—	0.94
4000	4100	E	0.197	2.27	11.5	—	3.04
4000	4180	D1	0.394	6.14	15.6	152	7.33

approach the value 1. Therefore, the expression for the net heat flux is dominated by the conduction terms

$$q(T) = -\left(\frac{\partial\theta_1}{\partial Z} + \frac{\partial\theta_2}{\partial Z}\right)_0. \tag{14}$$

It is noted that the above argument and the last relationship hold not only for steady states but for any transient too. For the former flow, the temperature derivatives can be calculated from equations (6a), yielding $(\mathrm{d}\theta_1/\mathrm{d}Z)_0 \to 0$ and $(\mathrm{d}\theta_2/\mathrm{d}Z)_0 \to -W$ when $W \gg 1$. Thus the general expression (14) for the heat flux approaches the result (13) for strong convection. The other limit of q, for conduction controlled processes where the velocity is small, can be found from the linear distributions (5)

$$q = 2, \quad W \to 0. \tag{15}$$

For stable periodic flows, the instantaneous heat flux removed from the source is given by equation (14). The long-term average is obtained by integration of $q(T)$ over a half cycle

$$\bar{q} = \frac{1}{(\tau/2)}\int_0^{\tau/2} q(T)\,\mathrm{d}T \equiv \frac{H}{\tau/2}. \tag{16}$$

A few results for q are presented in Table 2, for several periodic solutions in regions E and D1 of Fig. 3. As can be expected, the heat flux in the latter cases are much lower (by an order of magnitude or more) than those given by equation (13), $q = W$, for the corresponding steady states. The loop is capable of removing heat even in region E, where no steady flows exist. However, if it is required to transfer large amounts of heat, it would be necessary to control the Rayleigh numbers (raising R and/or lowering S), such as to bring the loop to a stable steady flow in region D or even A. It is noted that a finite disturbance would be needed to cause steady flow in region D1, while any perturbation to rest would lead to a convective solution in regions D2 and A.

The relative importance of the heat transfer mechanisms in the process of carrying energy between the source and sink has been obtained above: $q \to 2$ when conduction governs and $q \gg 2$ when convection dominates. As can be seen from Table 2, the role of convection becomes more significant as the thermal Rayleigh number R increases.

Another interesting result, also presented in Table 2, is the equivalent location at the end of one-half cycle, of a fluid particle which emerges from the bottom container at the moment when the velocity changes sign ($V = 0$)

$$Y = \int_0^{\tau/2} V(T)\,\mathrm{d}T. \tag{17}$$

In cases where $Y < 1$, as the middle one in Table 2, the fluid oscillates in the two channels and there are no particles which complete the path between the containers. For $Y > 1$ the quantity $Y-1$ is a measure of the fluid which does leave the heat source and enters into the sink during the half cycle. As can be seen, this value is small for low R and becomes larger at high thermal Rayleigh numbers. In fact, for the last case in Table 2 $Y-1$ is of the order of H which indicates strong convection heat transfer. The amplitude of the oscillation here is large: 26.83, meaning that during most of the time there is high velocity in the loop. For steady flows with large velocities $q = W$, as shown above. For the periodic flow, however, thermal inertia accounts for the difference between $Y-1$ and H.

6. SUMMARY

A numerical method was developed for simulating the transient flow, heat and mass transfer in a double diffusive natural circulation loop. A comprehensive analysis was performed, using the method, to study the system behaviour in all the stability regions of the four-parameter space: thermal and saline Rayleigh numbers R, S, Prandtl and inverse Lewis numbers, P and Q. These regions and the marginal lines separating them, see Fig. 3, were obtained analytically in ref. [12].

Two main types of transients were considered: a small perturbation to the rest state, NF, and transition from forced to natural circulation, FF. In all the numerous cases investigated, it was found that the general loop behaviour corresponds, indeed, to the mode relevant to the location of the state in the stability chart. The transients lead monotonically to the steady solution in the instability region A, above the monotonic marginal stability line, R_M, and to the rest state in the global stability region B, below either this line or the OMSL, R_O. The decay to rest is either monotonic or oscillatory, depending on the vicinity of the state to these lines. The subcritical region C is below R_M or both R_M and R_O and above the critical line R_C, where two pairs of steady-state solutions exist: stable $\pm W$ and unstable $\pm \tilde{W}$. Here NF tran-

sients and FF for which the initial velocity, U, is smaller than $\tilde{W}$, decay to rest either monotonically or periodically. For $U > \tilde{W}$ one of the steady solutions is always established. A similar behavior is observed in D1, which is a sub-zone of the supercritical region D, except that here transients with $U < \tilde{W}$ lead to stable periodic solutions. For other initial conditions, these flows are developed in regions C and D1 if during the oscillations the growing amplitude does not reach $\tilde{W}$. In sub-zone D2 oscillatory and then monotonic transients carry the loop to either one of the steady solutions $\pm W$, depending on the initial conditions. In region E of the stability chart the rest state is unstable and no steady solutions exist; here all transients develop to stable periodic flows. For all cases investigated, no multiple long-term oscillatory solutions were found in regions D1 and E.

The results show that in all cases either one of the three long-term stable situations are established: rest (conduction) state, steady flow ($\pm W$) or periodic solution with constant amplitude and frequency, which are not monochromatic. No chaotic situations have been discovered for this loop, probably because there does not exist any case where an unstable solution appears without a corresponding stable one.

The trend of the constant frequencies, see Fig. 14, is to increase when raising S and lowering R (and also when P and Q decrease). ω changes continuously with these parameters in the whole range, including variations of crossing marginal and critical stability lines.

Results for the heat transfer in the loop show that for low driving forces, represented by the difference $R-S$ of the Rayleigh numbers, the heat transfer is conduction controlled, while convection dominates for large values. A criterion for estimating the importance of the two mechanisms was found, based on the value of the dimensionless heat flux: $q \to 2$ in the former case and $q \to W$ in the latter. The loop is capable of removing heat from the source to the sink even during the periodic flow. Obviously, the heat transfer is much lower, then, than that at steady flow.

The Rayleigh numbers in practical loops such as geothermal systems or reactor cooling cycles will be large, e.g. 10^8 and more. As can be seen from Fig. 3, the subcritical region C is quite narrow, and shrinks at smaller R and S when Q increases, cf. refs. [12, 13]. However, all other stability regions A, B, D, E may be encountered, with the general patterns shown and discussed above, where for large R and S the shape of the oscillations becomes more skewed. System design and control is needed in order to establish the desired state, e.g. stable steady flow or rest state. The inverse Lewis number, Q, varies in a wide range for various component combinations. For salts in water $Q \approx 100$ or more; for gas–gas mixtures $Q \approx O(1)$, e.g. 1.35 for air–CO_2, 2.5 for air–benzene and 0.54 for air–hydrogen; for liquid–liquid pairs the variation is larger, e.g. 0.066 for water–HCl and 150 for water–ethanol.

It is finally noted that all the present results show that the stability regions A–E exist for all the many values of P and Q studied. The patterns of flow within each region were found to be similar; different values of the parameters R, S, P and Q only change the magnitudes of the dependent variables and the location of the marginal lines in the stability chart.

REFERENCES

1. Y. Zvirin, A review of natural circulation loops in pressurized water reactors and other systems, *Nucl. Engng Des.* **67,** 203–225 (1981).
2. R. Greif, Natural circulation loops, *J. Heat Transfer* **110,** 1243–1258 (1988).
3. J. B. Keller, Periodic oscillations in a model of thermal convection, *J. Fluid Mech.* **26,** 599–606 (1966).
4. P. Welander, On the oscillatory instability of a differentially heated fluid loop, *J. Fluid Mech.* **29,** 17–30 (1967).
5. A. Mertol, R. Greif and Y. Zvirin, The transient, steady-state and stability behavior of a natural convection loop with a throughflow, *Int. J. Heat Mass Transfer* **24,** 621–633 (1981).
6. J. E. Hart, A new analysis of a closed loop thermosyphon, *Int. J. Heat Mass Transfer* **27,** 125–136 (1984).
7. M. Sen, E. Ramos and C. Treviño, The toroidal loop with known heat flux, *Int. J. Heat Mass Transfer* **28,** 219–233 (1985).
8. Y. Zvirin, The onset of flows and instabilities in a thermosyphon with parallel loops, *Nucl. Engng Des.* **92,** 217–226 (1986).
9. W. L. Siegmann and L. A. Rubenfeld, A nonlinear model for double-diffusive convection, *SIAM J. Appl. Math.* **29,** 540–557 (1975).
10. L. A. Rubenfeld and W. L. Siegmann, Nonlinear dynamic theory for a double-diffusive convection model, *SIAM J. Appl. Math.* **32,** 871–894 (1977).
11. J. E. Hart, A model of flow in a closed-loop thermosyphon including the Soret effect, *J. Heat Transfer* **107,** 840–849 (1985).
12. Y. Zvirin, Instabilities in a double-diffusive thermosyphon, *Int. J. Heat Mass Transfer* **30,** 1319–1329 (1987).
13. Y. Zvirin, Transient and stability phenomena in a double diffusive natural circulation loop, EEC-164, Energy Engng Center, Faculty of Mech. Engng, Technion, I.I.T., Haifa, Israel (July 1989).
14. S. Lifshitz and Y. Zvirin, Transient heat transfer in a double-diffusive thermosyphon, *Proc. Israel Conf. on Mech. Engng*, Haifa (May 1990).
15. A. Mertol, R. Greif and Y. Zvirin, Two dimensional analysis of transient flow and heat transfer in a natural circulation loop, *Wärme- und Stoffübertr.* **18,** 89–98 (1984).

PHENOMENE VARIABLE ET STABILITE DANS UNE BOUCLE DE CONVECTION NATURELLE DOUBLEMENT DIFFUSIVE

Résumé—On applique une méthode numérique pour étudier les caractéristiques variables et stables d'une boucle de convection naturelle doublement diffusive. Le comportement de l'écoulement dépend de quatre paramètres d'espace et de propriétés; les nombres de Rayleigh thermique et salin R et S, ainsi que le nombre de Prandtl P et l'inverse de nombre de Lewis Q. Le diagramme de stabilité dans cet espace comprend cinq régions principales; des résultats numériques sont présentés pour des écoulements dans chacune d'elles. L'état de repos est aussi établi dans la région subcritique si la vitesse initiale est plus petite que la valeur critique, sinon on atteint un écoulement permanent. Dans la région supercritique, des solutions périodiques stables sont établies à la place de l'état de repos et dans la région périodique la boucle atteint toujours des oscillations stables à partir de conditions initiales quelconques. La fréquence des oscillations augmente avec S et diminue quand R, P et Q croissent. Le transfert de chaleur dans la boucle est étudié et on trouve que de la chaleur peut être évacuée pendant l'écoulement périodique établi.

INSTATIONÄRE ERSCHEINUNGEN UND STABILITÄTSPROBLEME IN EINER SCHLEIFENANORDNUNG BEI DOPPELT-DIFFUSIVER NATÜRLICHER ZIRKULATIONSSTRÖMUNG

Zusammenfassung—Instationäre Erscheinungen und Stabilitätsprobleme in einer Schleifenanordnung bei doppelt-diffusiver natürlicher Konvektionsströmung werden ausführlich numerisch untersucht. Das Strömungsverhalten im System hängt von dessen Zustand ab, der durch 4 Parameter definiert ist. Die temperaturbedingte und die konzentrationsbedingte Rayleigh-Zahl (R, S), die Prandtl-Zahl (P) und die inverse Lewis-Zahl (Q). Die Stabilitätskarte in diesem 4-Parameter-Raum, die bereits früher ermittelt wurde, enthält 5 Hauptbereiche. Die hier vorgestellten numerischen Ergebnisse decken jeden dieser Bereiche ab. Die zeitlichen Entwicklungen nähern sich monoton oder periodisch stabilen stationären Zuständen an, nämlich konvektionsbestimmten Strömungen oder ruhenden Zuständen mit Wärmeleitung jedoch ohne Strömung jeweils in den monotonen und insgesamt stabilen Gebieten. Der Ruhezustand stellt sich auch im unterkritischen Gebiet ein, wenn die Anfangsgeschwindigkeit kleiner als eine kritische Geschwindigkeit ist. In anderen Fällen ergibt sich eine stationäre Strömung. Im überkritischen Bereich ergeben sich stabile periodische Lösungen statt des Ruhezustandes, im periodischen Bereich erreicht die Schleife immer solche stationären Oszillationen, unabhängig vom Ausgangszustand. Die Frequenz der Oszillationen nimmt mit S zu, mit R, P und Q jedoch ab. Die Wärmeübertragung in der Schleifenanordnung wird ebenfalls untersucht. Dabei zeigt sich, daß bei der stabilen periodischen Strömung etwas Wärme abgeführt werden kann.

ПЕРЕХОДНЫЕ ПРОЦЕССЫ И УСТОЙЧИВОСТЬ В КОНТУРЕ ЕСТЕСТВЕННОЙ ЦИРКУЛЯЦИИ С ДИФФУЗИЕЙ ТЕПЛА И МАССЫ

Аннотация—Численно исследуются переходные характеристики и параметры устойчивости контура естественной циркуляции с диффузией тепла и массы. Поведение течения в системе зависит от положения в четырехпараметрическом пространстве тепло- и массообменного чисел Рэлея R, S, а также числа Прандтля и обратной величины числа Льюиса P, Q. Полученная ранее карта устойчивости в данном пространстве включает пять основных областей. Представлены численные результаты для течений в каждой из них. Переходные состояния монотонно или периодически приближаются к устойчивым стационарным состояниям конвективных течений или кондуктивных состояний покоя без течения в монотонной и глобальной областях устойчивости соответственно. Состояние покоя также устанавливается в субкритической области, если начальная скорость меньше критической, в противном случае имеет место стационарное течение. В закритической области вместо состояния покоя появляются устойчивые периодические решения, и в этой области при любых начальных условиях контур приходит в состояние таких устойчивых колебаний. Частота колебаний увеличивается с ростом величины S и уменьшается с убыванием величин R, P и Q. Исследуется также теплоперенос в контуре, и установлено, что при устойчивом периодическом течении некоторое количество тепла может отводиться.